Conformational Flexibility and Self-Association of Fibrinogen in Concentrated Solutions

Yuriy F. Zuev,*,[†,‡] Rustem I. Litvinov,[§,‡] Alexander E. Sitnitsky,[†] Bulat Z. Idiyatullin,[†] Dilyafruz R. Bakirova,[†] Dennis K. Galanakis,[⊥] Artem Zhmurov,[#] Valeri Barsegov,[∥,#] and John W. Weisel*,[§]

[†]Kazan Institute of Biochemistry and Biophysics, 420111 Kazan, Russian Federation
[‡]Kazan Federal University, 420000 Kazan, Russian Federation
[§]Perelman School of Medicine, University of Pennsylvania, Philadelphia, Pennsylvania 19104, United States
[⊥]SUNY at Stony Brook School of Medicine, Stony Brook, New York 11794, United States
[∥]Department of Chemistry, University of Massachusetts, Lowell, Massachusetts 01854, United States
[#]Moscow Institute of Physics & Technology, 141701 Moscow Region, Russian Federation

ABSTRACT: We studied the hydrodynamic behavior of fibrinogen, a blood plasma protein involved in blood clotting, in a broad 0.3−60 mg/mL range of concentration and 5−42 °C temperature using pulsed-field gradient ^{1}H NMR-diffusometry. Arrhenius plots revealed the activation energy for fibrinogen diffusion E_d = 21.3 kJ/mol at 1.4 mg/mL and 28.4 kJ/mol at 38 mg/mL. We found a dramatic slowdown in fibrinogen self-diffusion with concentration beginning at 1.7−3.4 mg/mL, which deviated from the standard hard-particle behavior, suggesting a remarkable intermolecular entanglement. This concentration dependence was observed regardless of the absence or presence of the GPRP peptide (inhibitor of fibrin polymerization), and also in samples free of fibrin oligomers. By contrast, diffusivity of fibrinogen variant I-9 with truncated C-terminal portions of the Aα chains was much less concentration-dependent, indicating the importance of intermolecular linkages formed by the αC regions. Theoretical models combined with all-atom molecular dynamics simulations revealed partially bent fibrinogen solution conformations that interpolate between a flexible chain and a rigid rod observed in the crystal. The results obtained illuminate the important role of the αC regions in modulating the fibrinogen molecular shape through formation of weak intermolecular linkages that control the bulk properties of fibrinogen solutions.
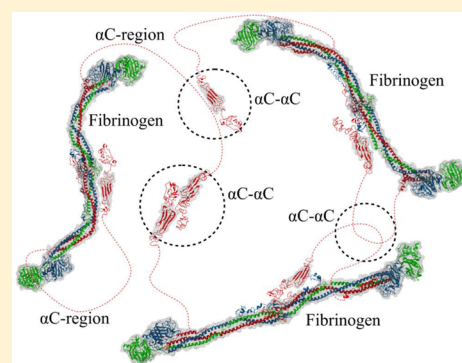
■ INTRODUCTION

Fibrinogen (Fg) is a soluble protein normally present in human blood plasma at a concentration of about 2.5−4 mg/mL forming an insoluble clot or gel after proteolytic conversion to fibrin.[1] A viscoelastic fibrin clot is necessary to prevent blood loss and promote wound healing. In surgery, fibrin sealants are formed from concentrated (up to 60 mg/mL) Fg followed by application to a bleeding wound to achieve hemostasis.[2] Fg might polymerize without proteolytic action,[3] but the (patho)-physiological implications of this phenomenon are unclear. Due to various functions in blood clotting, Fg molecules are also involved in many intermolecular interactions and, therefore, the physical molecular characteristics of Fg are of paramount importance for biology and medicine.

Transmission electron microscopy and X-ray crystallography data demonstrate that the Fg molecule has an elongated shape 45 nm in length and ~2−3 nm in diameter.[4−11] Each molecule has two distal and one central globular parts connected by two 17 nm-long triple and partially quadruple α-helical coiled-coils (Figure 1). In addition, there is a relatively unstructured part extending from the distal coiled-coil of each Aα chain named the αC regions (residues Aα221−610 in human Fg), comprising about 25% of the mass of the molecule.[12] The C-termini of the Aα chains have been visualized using the transmission electron microscopy[13] and atomic force micros-copy.[14] The two αC regions of Fg interact with each other and associate with the central region of the molecule, but there is a great conformational change that occurs to fibrin when the αC regions dissociate, thereby moving away from the molecular backbone and thus becoming available for intermolecular contact formation.[15] Yet, the intra- and intermolecular interactions of the αC regions in Fg are relatively weak,[16] and so they could mediate only unstable, short-lived Fg multimolecular contacts in solution. It has been demonstrated that the truncation of the αC regions affects the hydrodynamic behavior of Fg in dilute solutions.[17]

Apart from the role of Fg in blood clotting, molecular characteristics of Fg, a large multimeric protein with a complex
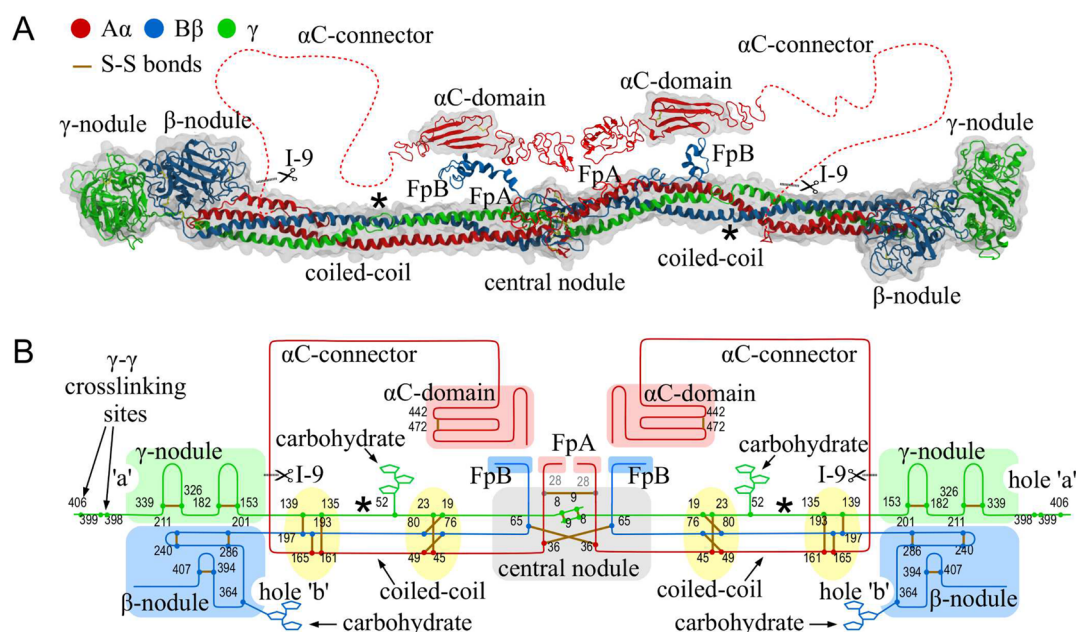
Figure 1. Human fibrinogen structure (PDB entry: 3GHG; color denotation is presented on the figure). (A) Structural details showing the central nodule, γ-nodules, β-nodules, disulfide rings, αC-connectors, αC-domains, and fibrinopeptides A (FpA) and B (FpB). The fibrinogen molecule is shown as in the compact crystal structure, with the truncation sites for I-9 fibrinogen variant indicated by the scissors. Addition of flexible C-terminal portions of the Aα chains (αC regions) is reconstructed computationally with respect to the NMR structure of isolated αC domains[32,53] and the high-resolution atomic force microscope images of Fg.[14] The extended αC regions are necessary to account for the hydrodynamic properties of Fg molecule.[17] (B) A schematic representation of the fibrinogen molecule in the naturally folded state with the addition of γ−γ cross-linking sites and carbohydrate moieties. The schematic also shows location of holes "a" and holes "b" in the γ-nodules and β-nodules, respectively. Both panels also show the location of the cleavage site for the I-9 variant of fibrinogen (scissors) and the location of the plasmin cleavage site, which coincide with the flexible hinge in the central part of the coiled coils (asterisk).

structure and intrinsic conformational flexibility, are of fundamental biological importance. Studies of solution properties of Fg have been ongoing for years,[17−21] but they all were performed in diluted solutions. However, it should be expected that in more concentrated solutions a highly elongated and flexible Fg molecule can deviate from hydrodynamic characteristics of the standard Stokes−Einstein description. Moreover, the hydrodynamic behavior of Fg might be even more complex, especially at high protein concentrations, due to sticky, extremely flexible, and largely unstructured ∼390-residue long appendages comprised by the αC regions (Figure 1).

Here, we performed direct hydrodynamic characterization of Fg using the Fourier-transform pulsed-gradient spin−echo NMR (PFG NMR) to measure a spontaneous displacement of molecules in the absence of a concentration gradient, characterized by a self-diffusion coefficient.[22,23] This methodology has been widely used to investigate protein structure and solution properties, including self-association and aggregation.[23,24] Because the self-diffusion coefficient D describes the motion of a single macromolecule in solution and characterizes the flow of solute particles relative to each other, it depends both on the particle−solvent and on the particle−particle friction coefficients. Hence, at the molecular level the diffusion coefficient can be related to the size and shape of the solute particles and the strength of intermolecular interactions. There was a single study in which the NMR-based methodology was applied to determine the Fg self-diffusion coefficient.[25] However, those experiments were carried out using nonselective NMR in uncharacterized samples of plasma and whole blood clots, for which the assignment of data to a particular protein is problematic.

In this work, we have characterized the bulk physical properties of purified Fg in a broad range of protein concentrations (0.3−60.0 mg/mL). Our studies show rich hydrodynamic behavior of Fg in solution environment, including the unusual, rapid decrease in molecular diffusivity of Fg with concentration. Analysis of experimental data revealed a remarkable intermolecular entanglement effect due to formation of noncovalent linkages coupling Fg into a dynamic matrix of self-assembled Fg molecules. Theoretical modeling of the experimental data has enabled us to gather information about the Fg molecular size and shape and quantitative parameters of hydrodynamic behavior of Fg molecules in semidilute to concentrated solutions. We used the all-atom molecular dynamics (MD) simulations of Fg molecule to link the bulk physical properties of Fg to its structural characteristics at the molecular level. The results obtained indicate that Fg conformations in solution are likely to interpolate between flexible and rod-like shapes with a high degree of molecular flexibility. We propose a model that considers the propensity of Fg to engage in noncovalent long-range intermolecular interactions through highly extendable unstructured αC regions. The results illuminate an important role played by the αC regions in determining the hydrodynamic properties of Fg in concentrated solutions.

■ MATERIALS AND METHODS

Handling and Characterization of the Full-Length Fg. Fresh protein samples for the NMR measurements were prepared from lyophilized bovine (Calbiochem, USA) or human (HYPHEN Biomed, France) Fg. The powder was dissolved in 150 mM NaCl at 37 °C at increasing

concentrations up to the point of saturation, then Zeba spin desalting columns with 7K MWCO (Thermo Fisher Scientific, Waltham, MA) were used to get rid of low-molecular weight stabilizers and preserving agents and to transfer the protein into 20 mM Tris-HCl buffer, pH 7.4, containing 150 mM NaCl. After centrifugation at 20 000g and 4 °C for 15 min to remove all microprecipitates, the Fg concentration was determined by absorbance at λ = 280 nm using an extinction coefficient of 1.51 for 1 mg/mL in a 1 cm cuvette. To exclude possible effects of potentially contaminating fibrin oligomers, we obtained fibrin-depleted human Fg preparation from the Fg subfraction I-2 purified from blood plasma.[26] Prior to depletion of its soluble fibrin oligomers, human Fg I-2 was treated with 200 nM PMSF to neutralize possible trace protease contaminants. Such preparations were dialyzed against 50 mM NaH$_2$PO$_4$ at 4 °C and the resulting polymers were removed. The supernatant Fg was precipitated with 26% saturated (NH$_4$)$_2$SO$_4$, dissolved in phosphate-buffered saline and dialyzed against 50 mM NaH$_2$PO$_4$ at 4 °C. Minor amounts of polymer formed at each step were also removed. The maximum Fg concentration obtained was 60 mg/mL (176 μM) for bovine and 42 mg/mL (123 μM) for human Fg. All the full-length Fg preparations were 93−95% pure, as determined using 7% SDS-PAGE in reducing and nonreducing conditions, and 95−97% clottable by thrombin, indicating that Fg was fully functional.

Purification and Characterization of Human Fg Subfraction I-9. A thrombin-coagulable catabolic subfraction, Fg I-9 (des-αC Fg) comprises a minor part of circulating plasma Fg.[27] This subfraction lacks the C-terminal portion of its Aα chain corresponding to a major part of its αC region (residues 221−610)[26] and contains the Aα chain core remnants ranged from 46.5 kDa to 22.6 kDa (Figure 2). As estimated from these measurements, this subfraction lacks virtually all of the αC-domains (Aα392−610) and variable lengths of the αC-connector (Aα221−391). Evaluated by SDS-PAGE, the Bβ and γ chains of I-9 were intact (Figure 2). To remove possible contaminations of monomeric and/or oligomeric fibrin, the Fg I-9 preparation used in this study was modified by including a
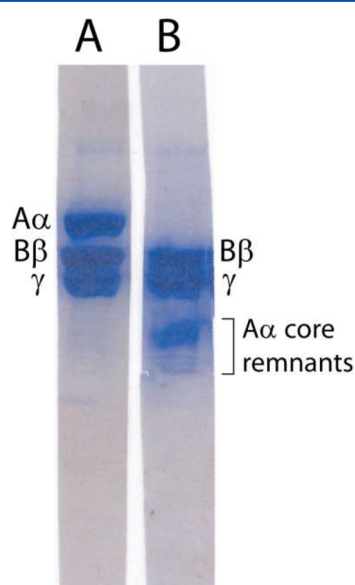

Figure 2. SDS-PAGE in reducing conditions showing the polypeptide chain composition of the full-length human Fg (A) and truncated Fg I-9 without the αC regions (B).

final dialysis step in 50 mM NaH$_2$PO$_4$ at 4 °C. The resulting spontaneously formed precipitates, representing ~6% of total Fg and containing a minor population of molecules (≤5%) possessing intact Aα chains, were removed. For NMR experiments Fg I-9 was transferred into 20 mM Tris-HCl buffer, pH 7.4, containing 150 mM NaCl, using Zeba desalting columns. Because of the extremely low yield of fibrin-depleted Fg I-9 (about 1% of total Fg present in human plasma), the concentration of Fg I-9 used in this study was only up to 4.5 mg/mL (~13 μM).

Self-Diffusion Measurements by NMR Gradient Technique. The main ^{1}H NMR experiments were carried out on a Bruker AVANCE III NMR spectrometer operating at 600.13 MHz equipped with a standard z-gradient inverse probe head (TXI, 5 mm tube) capable of producing gradients with a maximum strength of 55.7 G/cm. We used a stimulated-echo sequence incorporating bipolar gradient pulses and a longitudinal eddy current delay (BPP-LED).[28] The water signal was suppressed by means of presaturation. The following experimental parameters were used: a 90° pulse length 10−15 μs; spectral width 16 ppm; time domain data points 16−32 K; the number of scans 8; recycling delay 2−5 s. The amplitude of field gradient was varied from 2% to 95% of its maximum value over 16−32 increments under constant diffusion time (50 ms) and gradient pulse duration (8−12 ms). A gradient recovery delay of 0.1 ms and an eddy current delay of 5 ms were used. Data processing and the analysis were performed using the Bruker Topspin 2.1 software. As the samples were prepared in a nondeuterated solvent, the NMR spectra and self-diffusion measurements were recorded in the "unlocked" mode (the "lock" turned off).[29] The chemical shift region 0.9−0.6 ppm for measurement of the self-diffusion coefficient was chosen in the upfield domain of the spectrum that encompassed strong signals for Fg methyl protons (Figure 3). This region was selected to eliminate potential errors in the peak integrals arising from disturbances of the water signal in the spectrum and to avoid extra complications from overlapping signals. A DOSY (diffusion-ordered spectrocopy) spectrum (Figure 3) depicts that all protein signals give the only value of the self-diffusion coefficient. The measurements were performed at 37 °C unless otherwise indicated. Control measurements performed with PFG NMR for a number of well-characterized proteins (bovine serum albumin, lysozyme, trypsin, and chymotrypsin) provided values for the self-diffusion coefficients that are either consistent with the literature and structure-based predictions or higher by 10−20%, suggesting the existence of a method-dependent variability of the apparent protein diffusivity.

Viscosimetry. Viscosity of solutions was determined using a rolling-ball viscometer, Anton Paar Lovis 2000 ME, which measures the rolling time of a ball through transparent and opaque liquids according to Hoeppler's falling ball principle. Results are given as dynamic viscosity. The instrument was calibrated with water following the instructions and requirements of the manufacturer. The temperature 37 °C was controlled by the built-in Peltier thermocouple within ±0.02 °C. The viscosity measurements of each sample were made in triplicate with accuracy within 0.5% variation.

In Silico Modeling. The atomic model of the full-length Fg molecule was constructed using a crystal structure of human Fg (PDB code: 3GHG).[7] The following missing residues unresolved in the crystal structure were synthesized *in silico* and incorporated into the structure using the VMD
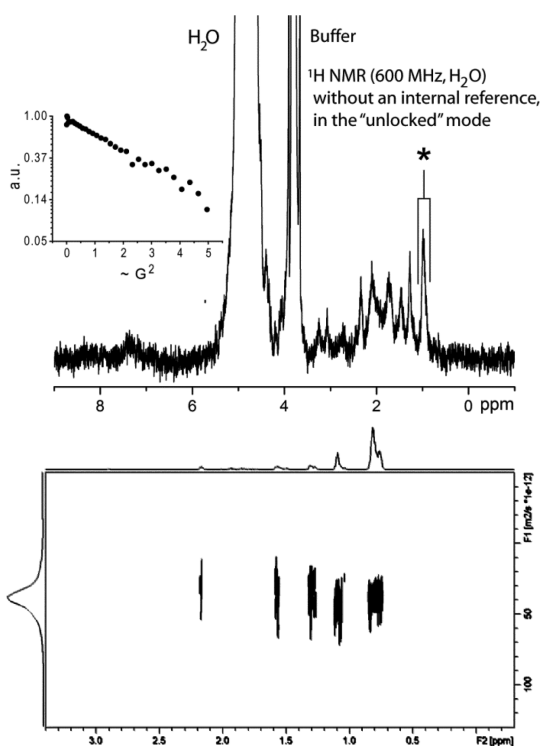
Figure 3. Top: ^1H NMR spectrum of human Fg at 37 °C. The signal used for diffusion measurements is marked by an asterisk. The insert shows the diffusive decay of this signal. Bottom: DOSY spectrum of human Fg at 37 °C (see Materials and Methods).

Molefacture plug-in:[30] (i) $A\alpha1-26$ (fibrinopeptide A, $A\alpha1-16$, followed by the knob "A"-containing motif); (ii) $B\beta1-57$ (fibrinopeptide B, $B\beta1-14$, followed by the knob "B"-containing motif); (iii) $B\beta459-461$ (the C-terminal end of the $B\beta$ chain); (iv) $\gamma1-13$ (the N-terminal part of the γ chain); and (v) $\gamma395-411$ (the C-terminal end of the γ chain containing the $\gamma-\gamma$ cross-linking site). We also added (vi) residues $A\alpha201-610$ to the full-length Fg molecule and $A\alpha201-221$ to the Fg I-9 variant. The structure of the αC-domain (residues $A\alpha392-610$, Figure 1) was constructed with the Modeler program[31] using sequence homology with the partly resolved structure of the bovine αC-domain (PDB code: 2JOR).[32] Each system was energy-minimized using the steepest descent algorithm, and heated to 37 °C and equilibrated for 10 ns. We carried out long 1-μs MD simulations at 37 °C using the solvent accessible surface area (SASA) model of implicit solvation.[33,34] The simulation output was used in subsequent structure analysis and visualization.

Molecular Models of Fg in Solution. To link the experimentally measurable bulk physical properties of Fg solutions with a molecular size of the protein, we employed the following analytically tractable models linking the diffusion coefficient $D = k_BT/f(L)\eta$ and solution viscosity η (see eq 5):

(i) Brownian spherical particle of size (radius) $L = R_s$:

$$f(R_s) = 6\pi R_s \text{ and } D_s = k_BT/6\pi R_s\eta \quad (1)$$

(ii) Brownian rod-like particle with length l and width of cross-sectional area w:

$$f_r(l, w) = 3\pi l/\ln[l/w] \text{ and } D_r = k_BT\ln[l/w]/3\pi l\eta \quad (2)$$

(iii) Rouse chain of n connected beads of size b with total size $L = bn$:

$$f_R(b, n) = bn \text{ and } D_R = k_BT/bn\eta \quad (3)$$

(iv) and Zimm polymer of size $L_Z \approx bn^v$ ($v = 0.588$):

$$f_Z(b, n) = [3(6\pi^3)^{1/2}/8]bn^v \text{ and } D_Z$$
$$\approx 0.196 k_BT/bn^v\eta \quad (4)$$

In eqs 1−4 above, T is the absolute temperature and k_B is Boltzmann's constant. In the Brownian models, the diffusive motion is due to displacements of particles in a surrounding liquid due to random collisions with water molecules. Both Brownian spherical particle (i) and Brownian rod-like particle (ii) models have the correct physical picture for the intrinsic viscosity, if the collapsed biopolymer can be treated as a spherical blob or a cylinder (eqs 1 and 2). Hence, a disagreement between the Brownian model-based predictions on Fg size and the X-ray structure would imply deviation of the solution structure from the spherical or cylindrical shape. In the Rouse model (iii), the beads roughly represent the distal and central globular parts connected by the coiled-coils. In our previous study of the Fg molecule in solution, we showed that the coiled-coil connectors behave as entropic springs.[34,35,36] In the Rouse model, each bead is characterized by its own friction (see eq 3), and water molecules drain freely through a moving protein chain. Because the Rouse model ignores hydrodynamic interactions of a biopolymer chain with solvent and neglects the intrinsic viscosity $[\eta]$, a disagreement between the model predictions and the crystal structure would imply the importance of hydrodynamic coupling. By contrast, the Zimm model (iv) assumes that a biopolymer of size bn^v drags surrounding water molecules contained within its pervaded volume, i.e. the volume of solution spanned by the polymer chain. The Zimm model considers hydrodynamic interactions of Fg chain with water molecules and it has the correct physical picture for the intrinsic viscosity (eq 4).

RESULTS

Temperature Dependence of Fg Self-Diffusion. First, we explored the dependence of Fg diffusivity on temperature. Figure 4 shows the D/D_0 values for Fg and water as a function of the inverse temperature in the 5−42 °C range. The diffusivity of both solute and solvent exhibits a typical Arrhenius behavior. The measurements have shown the batch- and species-independence; the bovine and human Fg preparations gave very similar results. The extracted value of activation energy for Fg self-diffusion, $E_d = 21.3$ kJ/mol in 1.42 mg/mL Fg solution, agrees well with 18.0−20.4 kJ/mol determined earlier for water in a protein (lysozyme) solution[36] at the equivalent protein concentrations. For comparison, the activation energy for self-diffusion of pure water is $E_W = 17.8$ kJ/mol.[37] In Figure 4 the slopes of the dependence of self-diffusion on the inverse temperature for the full-length Fg (1.3−1.4 mg/mL) correspond to the value of viscous flow of a protein characterized by minimal protein−protein interactions with an activation energy of $E_W = 22.0$ kJ/mol. The diffusive motion of Fg in concentrated solution (38.3 mg/mL) showed an increase of the activation energy to $E_d = 28.4$ kJ/mol, likely reflecting increasing interactions between the protein molecules.[24] Thus, the main conclusion is the following: in the 5−42
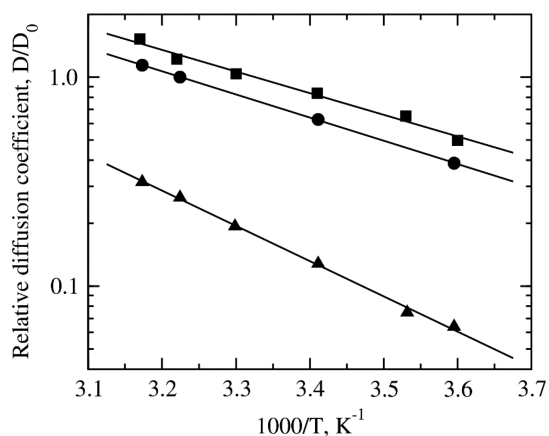
Figure 4. Arrhenius plots of the relative self-diffusion coefficients (D/D_0) of water (circles) and full-length human Fg in 1.4 mg/mL Fg solution (squares) and in 38.3 mg/mL Fg solution (triangles) in a physiological buffer.

°C temperature range at a physiological ionic strength (150 mM NaCl) and pH 7.4, there were no visible changes in the hydrodynamic properties of Fg, implying that Fg solutions remained thermally stable in the 5−42 °C temperature range. Importantly, this range is used for *in vitro* studies and when handling Fg concentrates clinically used for infusion or for local applications to form a fibrin sealant to stem bleeding.

Dependence of Fg Self-Diffusion on Protein Concentration. Next, we studied the Fg hydrodynamics in a broad range of protein concentrations. Figure 5 shows the depend-
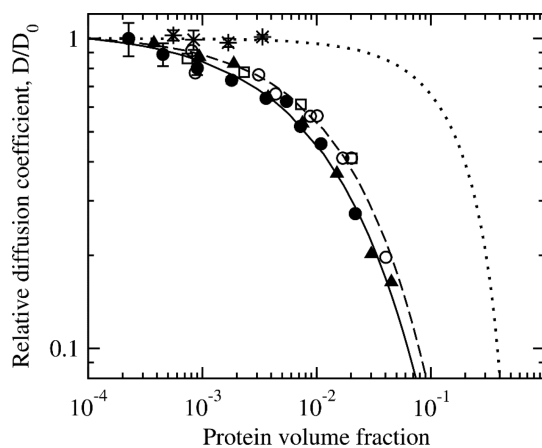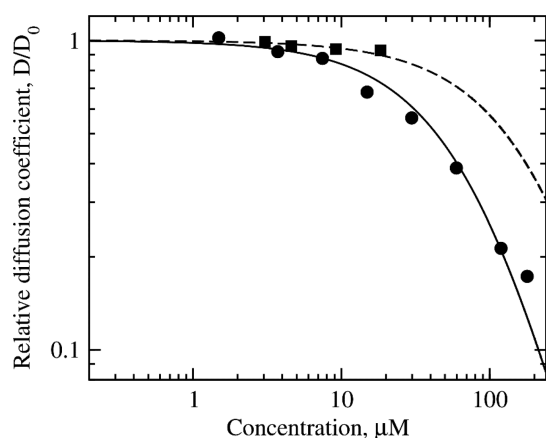

Figure 5. Log−log plot of relative self-diffusion coefficient D/D_0 as a function of protein volume fraction for the full-length bovine Fg (triangles), human Fg (dark circles), fibrin-depleted human Fg (squares), bovine Fg in the presence of the GPRP peptide (open circles), and truncated human Fg I-9 (stars) in a physiological buffer (150 mM NaCl, pH 7.4) at 37 °C. The solid and dashed lines are the fitting curves obtained using a generic stretched exponential function just to guide the eye, while the dotted line is a prediction for hard nonaggregating particles by Tokuyama and Oppenheim.[41]

ence of self-diffusion coefficients on protein volume fraction for all Fg preparations studied in an experimentally accessible concentration range at 37 °C, pH 7.4, and physiological ionic strength of 150 mM NaCl. To avoid possible complications related to method-dependence of D values, we analyzed the reduced self-diffusion coefficient D/D_0, where D_0 is the self-diffusion coefficient at the infinite dilution obtained by the

extrapolation of the D values using an exponential function. The protein volume fraction φ was calculated using the specific densities of 1.399 g/cm^3 for the full-length Fg and 1.391 g/cm^3 for Fg I-9.[19] In our experiments, the Fg concentrations spanned 2 orders of magnitude from 0.3 mg/mL up to 60 mg/mL (corresponding to the 2.4×10^{-4} and 4.6×10^{-2} volume fractions, respectively), which is a much broader range than the concentrations used in earlier studies. Our experiments revealed the large-scale concentration-dependent effects for the full-length Fg and the large changes in the translational diffusion observed at relatively low concentrations of 1.7−3.4 mg/mL (5−10 μM) (Figure 5). The diffusive mobility of Fg is dramatically reduced when the concentration reaches ∼60 mg/mL (180 μM). The diffusive mobility of bovine and human Fg was nearly indistinguishable (Figure 5), which agrees with the high degree of their structural similarity.[38] Hence, the results in Figure 5 clearly demonstrate that the diffusive mobility of full-length Fg undergoes a dramatic slow-down at essentially lower solution concentrations than predicted for hard-sphere particles.

Influence of Fibrin(ogen) Oligomeric Structures. To confirm that the observed steep decrease in Fg diffusivity was not due to potential contamination of commercial Fg preparations by oligomeric fibrin-Fg complexes, we employed two different approaches. In the first approach, we determined the self-diffusion coefficient of the purified full-length human Fg (subfraction I-2)[26] depleted of fibrin in the 1−27 mg/mL concentration range. The results presented in Figure 5 show that the values of self-diffusion coefficient for fibrin-depleted Fg I-2 are 10−25% higher than those for regular Fg at the corresponding concentrations, suggesting that only a minor fraction of oligomers was present in the full-length Fg preparations. The lack of fibrin oligomers did not change the overall shape of diffusion profile, implying that the diffusive mobility of full-length Fg drastically decreases with the increasing concentrations. The second approach was based on introducing the Gly-Pro-Arg-Pro (GPRP) peptide (Bachem Americas, Torrance, California, USA), a knob "A"-mimetic,[39] a highly specific competitive inhibitor of fibrin polymerization capable of depolymerizing un-cross-linked fibrin.[40] When GPRP was added to the bovine full-length Fg (up to a 50-fold molar excess of the peptide in the 1−54 mg/mL range of Fg concentration), the concentration dependence remained unchanged (Figure 5), although the values of self-diffusion coefficient were slightly higher, consistent with the presence of a minor fraction of fibrin oligomers in Fg preparations.[26] Hence, possible presence of fibrin oligomers did not alter the shape of the profile of Fg diffusivity vs concentration, thus implying that Fg self-diffusion is determined solely by the intrinsic properties of the Fg molecule.

Role of Flexible αC Regions. To determine whether the observed hydrodynamic behavior of Fg was due to the presence of αC regions, we next compared the concentration dependence of self-diffusion coefficients for full-length Fg versus Fg I-9 with truncated αC regions (des-αC Fg). Our results show that Fg I-9 and full-length Fg differ in the diffusive mobility pattern in the volume fraction range studied. The behavior of truncated Fg I-9 agrees with the predictions for hard spheres (Figures 5 and 6),[24,41] while the experimental data for the full-length Fg strongly deviate from this prediction. Although the concentration dependence of truncated Fg I-9 agrees with the hard-particle theory in the range of concentrations used in this work, the deviation might be observed at higher concentrations that

Figure 6. Numerical fit of the theoretical curves of relative self-diffusion coefficient (solid and dashed curves for the full-length Fg and truncated Fg I-9, respectively) to the experimental profiles (data points) of D/D_0 versus molar concentration C (circles for the full-length Fg and squares for the truncated Fg I-9). All four models of the Fg chain lead to similar fitting results, and so we only display the results for Zimm model.

were unachievable due to relatively small amount of Fg I-9 available. Therefore, the difference in the behavior of full-length Fg vs des-αC Fg illuminates the importance of the αC regions, a major structural determinant of Fg. Hence, the results obtained clearly demonstrate that the concentration dependence of molecular diffusion observed for full-length Fg is mainly due to protein−protein interactions mediated by the αC regions, i.e., extended appendages emanating outward from the folded part of Fg (Figure 1).

Viscosity-Related Effects on Fg Self-Diffusion. To determine whether the decrease in Fg self-diffusion with concentration was solely due to the increase in viscosity, we also measured the diffusive mobility of Fg in sucrose solutions. First, we determined the viscosity of a highly concentrated Fg solution (48 mg/mL), which came to the average value of 2.73 mPa·s. Using a table of sucrose viscosity,[42] we found that this value corresponds to the viscosity of a 36% sucrose solution. Next, we prepared a dilute Fg solution (1 mg/mL) in 36% sucrose and measured the self-diffusion coefficient of Fg in order to test whether the high viscosity affects the measured diffusivity of the protein. The results accumulated in Table 1 show that in the presence of 36% sucrose (i.e., at the viscosity

corresponding to the 48 mg/mL Fg solution) the self-diffusion of Fg at 1 mg/mL was reduced ∼2-fold but was still 2.7 times larger than that for a 48 mg/mL Fg solution with same viscosity. Hence, a significant decrease in Fg self-diffusion in more concentrated solutions cannot be attributed exclusively to the increase of solution viscosity.

Determination of Intrinsic Viscosity from Concentration-Dependent Diffusion of Fg. To analyze the experimental dependence of diffusion coefficient D in the entire range of Fg concentration, we invoked the Stokes−Einstein theory:
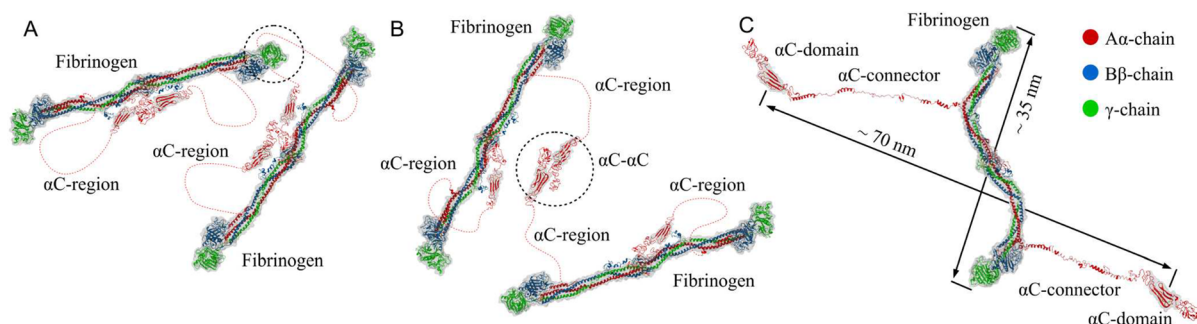
$$D = k_B T/\zeta = k_B T/f(L)\eta \tag{5}$$

In eq 5, the friction coefficient $\zeta = f(L)\eta$ depends on the solution viscosity η and protein size L; see eqs 1−4. The dependence of η on molar concentration C is given by[43]

$$\eta = \eta_s(1 + [\eta]C + k_H[\eta]^2 C^2) \tag{6}$$

where η_s is the solvent viscosity, $[\eta]$ is the intrinsic protein viscosity given in the units of reciprocal mass concentration, and k_H is the Huggins coefficient. Because the profiles of D versus C for the bovine and human Fg are very similar (Figure 5), here we analyzed the bovine Fg data only.

The profile of D versus C for the full-length Fg shows two distinctly different slopes which points to bimodal dependence (Figure 6). Therefore, we assumed that depending on concentration Fg molecule has two different conformational states, namely the compact state stable with collapsed α chains in a diluted solution and the extended state with elongated α chains which becomes increasingly more populated at a higher concentration. The transition from the compact state to the extended state occurs at the characteristic concentration $C = C^*$. Corresponding to the two-state model, the average intrinsic viscosity is given by $[\eta] = [\eta]_c p_c + [\eta]_e p_e$ where the populations of the compact and extended states are given by $p_c = 1/(1+\exp[-C/C^*])$ and $p_e = 1 - p_c$, respectively. By definition, intrinsic viscosity is a property in the limit of infinite dilution (zero concentration), but since intrinsic viscosity is a function of solute size and shape, if these change with concentration, so should intrinsic viscosity. To estimate $[\eta]$ and k_H, we performed a fit of the theoretical curves of relative diffusion coefficient D/D_0 (see eqs 5 and 6 above) to the experimental data for bovine Fg at 37 °C using D_0 at the infinite dilution for the full-length Fg and Fg I-9. We set $\eta_s = 0.69 \times 10^3$ kg m^{-1} s^{-1} and ignored the effect of 150 mM NaCl and buffer salts on water viscosity.[44] A visual comparison of the theoretical curve and experimental data points for D/D_0 versus C shows excellent agreement (Figure 6). The numerical values of intrinsic viscosity and Huggins coefficient obtained from the fit come to $[\eta]_c = 30.1$ cm^3/g (0.0105 L/μM) for the compact state and $[\eta]_e = 81.1$ cm^3/g (0.0275 L/μM) for the extended state, and $k_H = 0.49$. We found that the characteristic concentration is $C^* = 20$ mg/mL (60 μM). The extracted value of $[\eta]_c$ is comparable with the experimentally measured values of 25−27 cm^3/g for intrinsic viscosity of Fg.[45−49] The 10−20% deviation can be attributed to high magnetic field utilized in NMR, which was used here for the first time to study hydrodynamics of Fg.

To model the Fg I-9 variant, we assumed that the truncated fibrinogen molecule without the αC regions exists only in one state. We performed a numerical fit of the theoretical curves of relative diffusion coefficient to the experimental data for D/D_0 vs C for Fg I-9 at 37 °C (Figure 6). Corresponding to a much

Table 1. Dynamic Viscosity ($n = 3$) and Self-Diffusion Coefficient of Fg in Solutions With Various Protein Concentrations and Viscosity

sample	dynamic viscosity η, mPa·s	relative diffusion coefficient, D/D_0
Tris-HCl buffer, pH 7.4	0.726 ± 0.002	
Fb at 1 mg/mL	0.751 ± 0.002	0.82
Fb at 5.5 mg/mL	0.824 ± 0.002	
Fb at 8.9 mg/mL	0.918 ± 0.004	
Fb at 20 mg/mL	1.264 ± 0.051	
Fb at 48 mg/mL	2.725 ± 0.002	0.17
Fg at 1 mg/mL in 36% sucrose		0.45
sucrose 36%	2.73[a]	

[a]Taken from Asadi, 2007.

Figure 7. (A) and (B) Specific examples of the molecular entanglement involving structural elements of Fg molecule. (A): A nonspecific αC-αC entanglement due to αC-regions of two proximal Fg molecules locking the molecules together through excluded volume interactions. (B) A specific αC-αC interaction resulting in direct coupling of Fg molecules due to intermolecular interactions between the αC-domains. (C) An average solution structure of Fg monomer observed in 1-μs MD simulation run (see Materials and Methods). Fg's Aα, Bβ, and γ chains are shown in red, blue, and green, respectively. Hydrodynamic volume is depicted as transparent molecular surface (i) for parts that are resolved in X-ray crystallography (PDB code: 3GHG; residues Aα27−200, Bβ58−458, and γ2−395) and (ii) for N-terminal parts of the αC-domains (residues Aα425−503) that were reconstructed *in silico* using the NMR structures for bovine fibrinogen (PDB code: 2JOR).[32,53]

slower decrease in the diffusion coefficient, $[\eta]$ = 25.2 cm^3/g (0.007 L/μM) and k_H = 0.38 are smaller for truncated Fg I-9 compared to the full-length Fg. The results obtained clearly indicate that the intrinsic viscosity of Fg is largely determined by the αC regions and their spatial reorganization at a higher Fg concentration.

Molecular Parameters of Fg Extracted from Intrinsic Viscosity. We can link the values of $[\eta]$ for the full-length Fg and Fg I-9 to their physical dimensions, because in polymer physics $[\eta]$ is proportional to the inverse concentration of the chain in its pervaded volume V_p, (volume of solution spanned by the chain), and so V_p can be used to gain insight into molecular dimensions of Fg, determined largely by a flexible unstructured portion, such as the Fg's αC regions. Based on a difference between $[\eta]_c$ and $[\eta]_e$, the volume V_p spanned by the full-length Fg monomer in the compact and extended states come, respectively, to V_{pc} = 16.9 × 10^3 nm^3 and V_{pe} = 45.5 × 10^3 nm^3 per molecule, while for the Fg I-9 molecule V_{pI-9} = 14.1 × 10^3 nm^3. These values can be used to estimate the radii of pervaded volume spheres, which come to $R \approx$ 24.2 nm for Fg I-9, and $R \approx$ 25.6 nm and $R \approx$ 35.7 nm for the compact and extended states of full-length Fg, respectively. It is noteworthy that PFG NMR can provide values of protein diffusivity that are somewhat different from those determined with common hydrodynamic techniques [see, e.g., for bovine serum albumin, ref 24 vs ref 50]; therefore, the provided molecular parameters may be method-dependent. Nevertheless, our results imply that the αC regions play an important role in defining the molecular shape of Fg. Given the 45 nm extended structure of Fg in the crystal, these results suggest that the solution structure of Fg is different from the crystal structure (Figure 1) and it also alters with concentration. In semidiluted and concentrated solutions, Fg both with and without αC regions may adopt a partially bent conformation (see Figure 7C). The extent of potential bending is larger for the des-αC Fg variant, which implies that the αC regions enable partial elongation of Fg molecules in solution from 25.6 to 35.7 nm.

Molecular Parameters of Fg from Theoretical Models. Using eqs 1−4 (see Materials and Methods), we obtained the hydrodynamic radius-based estimates of molecular size L_h and shape V_h for the full-length Fg (in a conformation averaged between the compact and extended forms) and truncated des-αC Fg molecules in solution. For the spherical Brownian particle model, $L_h = R_s$ and V_h = (4/3) πR_s^3; for the Brownian rod-like particle, L_h is given by the length l and width w, and so $V_h = \pi l w^2 / 4$. For the Rouse and Zimm models, the size is calculated as $L_h = bn$ and bn^v, respectively, and the volume is given by $V_h = b^3 n$ and $b^3 n^v$, respectively. In the Rouse and Zimm models, we set n = 3, i.e., three beads representing the two distal globular regions (with the γ- and β-nodules at each end) and the central nodule of Fg. Numerical values of L_h and V_h obtained using all four models are accumulated in Table 2.

Table 2. Average Molecular Dimensions[a] of the Fg Variants Corresponding to the Brownian Spherical and Rod-like Particle Models, Rouse Chain Model, and Zimm Polymer Model

model	full-length Fg (with αC) L_h (l/w), nm; V_h, nm^3	truncated Fg I-9 (des-αC) L_h (l/w), nm; V_h, nm^3
Brownian spherical particle	7.5; 1564.1	5.7; 776.0
Brownian rod-like particle	45.1/2.0; 178.6	34.0/1.8; 96.4
Rouse chain	139.0; 298,402	109.1; 143,892
Zimm polymer	25.8; 4,718	21.8; 2,846

[a] L_h is the hydrodynamic radius-based estimate of molecular size and V_h is the hydrodynamic volume-based estimates of molecular dimensions. For the Brownian spherical or rod-like particles, we provide the particle hydrodynamic radius $L_h = R_s$ or length/width l/w; for the Rouse and Zimm models, we report size $L_h = bn$ and bn^v, respectively, and volume $V_h = nb^3$ and $n^v b^3$, respectively. Numerical values of these parameters were determined from the fit of theoretical curves of diffusion coefficient D (eqs 1−4) to the experimentally determined dependence of this quantity on the molar concentration C (Figure 6).

Unlike the molecular dimensions of Fg extracted from intrinsic viscosity, the parameters in Table 2 refer mostly to the core of Fg molecules without considering possible effects of the αC regions.

Molecular Dynamics Simulations of Fg in Solution. To further explore the behavior of Fg monomer with and without the αC region in solution on the atomic scale, we ran five 1-μs MD trajectories for the full-length Fg molecule and for the Fg molecule truncated at residue Aα211 (see Materials and Methods). Both structures showed a large degree of bending (Figure 7C), which is consistent with an earlier MD simulation study[51] and our own results of theoretical modeling (Table 2).

Due to bending, the effective length of Fg in solution is smaller (35−37 nm) compared to the crystal state (~44 nm). The length of the full-length molecule was slightly longer than that for the truncated variant (37 ± 2 nm versus 35 ± 2 nm, $p <$ 0.05), which is also consistent with our theoretical predictions (Table 2). Although the αC-connectors were not observed to form any globular structures, we detected transient α-helices (Figure 7C). We compared the snapshots of αC-domains from five MD runs, each of which can be divided into two subdomains: the N-terminal subdomain with the double β-hairpin, which is largely similar to the initial structure,[32,52] and the C-terminal subdomain. Although the C-terminal subdomains can form compact globules, they are largely unstructured as observed in our MD simulations, and they do not form stable secondary structure (Figure 7). This is consistent with our NMR data showing that only the N-terminal part of αC-domain is resolved.[32,53]

■ DISCUSSION

Solution Properties of Fg. We described the hydro-dynamic behavior of Fg at various temperatures and concentrations, from diluted solutions (0.3 mg/mL) to semidiluted and concentrated solutions (up to 60 mg/mL) at the physiological values of ionic strength and in a broad temperature range. The most important experimental findings are the following: (i) The full-length Fg displays a strong reduction of diffusive mobility with increasing concentrations, and this concentration dependence deviates dramatically from theoretical predictions for hard-sphere particles; (ii) Unlike the full-length Fg, a Fg variant with truncated αC regions (Fg I-9) displays a diffusive mobility pattern that agrees with the predictions for hard spheres, thus illuminating the role of the αC regions in the dramatic reduction of Fg diffusivity; (iii) The hydrodynamic behavior of full-length Fg is maintained after elimination or depolymerization of contaminating fibrin, suggesting that soluble fibrin oligomers are not responsible for the remarkable hydrodynamic properties; (iv) The observed reduction of diffusive mobility of Fg with concentration is only partially due to the increase in solution viscosity, implying that there are inherent structural properties of Fg defining its unusual hydrodynamic behavior; (v) The hydrodynamic behavior of Fg, especially at high concentrations, is largely determined by the intermolecular self-association of Fg molecules mediated by the highly flexible and extensible αC regions; (vi) The hydrodynamic properties of Fg do not undergo visible changes in the 5−42 °C temperature interval and within the concentration range used in this work.

Role of the αC Regions. In dilute solutions, Fg molecules are spatially separated and the protein−protein interactions are negligible. Hence, the solution viscosity is a linear function of the protein concentration C, i.e., $\eta = \eta_s(1+[\eta]C)$.[54] This implies that in the dilute solution regime the contribution from protein molecules is additive and solution viscosity η grows linearly with C above the solvent viscosity η_s. However, in semidilute solutions, the intermolecular interactions play an increasingly more important role, and η involves a quadratic term $k_H[\eta]^2C^2$ (see eq 6). This higher-order term accounts for the protein−protein interactions when Fg's polypeptide chains overlap. The characteristic concentration C*, at which the overlap starts playing a role and influences the hydrodynamic behavior of Fg, can be estimated from the condition:

$$R^3C^*N_A \approx 1 \qquad (7)$$

where $V_p \sim R^3$ is the pervaded volume. Taking the radius of pervaded volume R to be roughly equal to the size of the Fg molecule, i.e., $R \approx 30−40$ nm, we find $C^* \approx 25−65$ μM, which corresponds to the very low $(6.25−15.0) \times 10^{-3}$ protein volume fraction. The 60 μM value of C* obtained from the fit of theoretical curves to experimental data points is in the 25−65-μM range. The comparative experimental data for the full-length Fg and Fg I-9 with truncated αC regions show that for both Fg variants the self-diffusion coefficient decreases inversely quadratically in this concentration range, but the corresponding nonlinear slowdown in D/D_0 for the full-length Fg occurs at a much lower 1.7−3.4 mg/mL (5−10 μM) concentration (Figures 5 and 6). This result strongly confirms the role of αC regions in defining the unique hydrodynamic behavior of Fg in solution.[19,17]

Theoretical Predictions for Molecular Parameters of Fg in Solution. All four analytically tractable models (Table 2) produced a good fit, so in order to discriminate between the models we need to analyze model predictions of Fg size and shape (Table 2). The Brownian sphere model largely underestimates the size of both full-length and truncated Fg molecules and predicts too small hydrodynamic radii $R_s = 7.5$ nm and $R_s = 5.7$ nm, respectively. Indeed, a hypothetical globular protein with $M \approx 340\,000$ g/mol (as Fg) and average protein density of ~1.3 g/cm³ would occupy a hydrodynamic volume of 3960 nm³, which is much larger than $(4/3)\pi(7.5$ nm$)^3 = 1767$ nm³. Hence, the solution structure of Fg largely deviates from a spherical blob. The Brownian rod-like particle model predicts the length and width of the cross-sectional area of the molecule to be equal to $l = 45$ nm and $w = 2$ nm for full-length Fg and to $l = 34$ nm and $w = 1.8$ nm for the Fg I-9. These numbers for the full-length Fg agree with the X-ray crystallography data[7] (see Figure 1). The model also predicts a 11 nm-length difference between the full-length and truncated Fg molecules. Hence, this model also points to the role of the αC regions in modulating molecular size and shape of Fg. The Rouse chain model largely overestimates the dimensions of Fg molecule, i.e., $L_h = 139$ nm for the full-length Fg vs 109 nm for Fg I-9, which corresponds to unrealistic hydrodynamic volume $V_h = 298\,000$ nm³ for full-length Fg and 144 000 nm³ for Fg I-9. While it might be expected that V_p can exceed V_h by several orders of magnitude (as for Brownian rod-like particle), V_h cannot be larger than $V_p = 29.8 \times 10^3$ nm³. The Zimm model predicts the molecular size of 25.8 nm for full-length Fg vs 21.8 nm for Fg I-9, and $V_h = 4718$ nm³ for full-length Fg vs 2846 nm³ for Fg I-9, which are comparable with V_p. Hence, this model also predicts a 4 nm-size difference between the full-length and truncated Fg molecules. Taken together, the Brownian rod-like particle and Zimm models provide the most meaningful interpretation of the experimental data.

Molecular Flexibility and Intermolecular Entanglement of Fg in Solution. Our results indicate that the Fg solution structure interpolates between the rigid-rod and flexible chain conformations. Structure visualization and analysis of MD simulations have revealed that the Fg solution structure is more likely to be found in sigmoidal and bent rather than a rod-shaped straight conformation. These structures showed different extents of bending and an average end-to-end distance of ~35 nm (Figure 7C). Analytical models predict a 11 nm (Brownian model) and 4 nm (Zimm model) size difference for the full-length versus truncated Fg, which correlates with the 2-fold increase in V_p with the inclusion of the αC regions. Together two αC regions (780 residues) comprise only ~1/3

of amino acids of the full-length Fg molecule (Figure 1). Given that major portions of the αC regions remain unstructured (αC-connectors; 2 × 171 = 342 residues), an ~30% increase in the system size cannot account for the 2-fold increase in pervaded volume. Hence, the αC regions may not only increase the overall dimensions of the Fg molecule, but also modulate its shape. Indeed, at ~10 μM concentration Fg monomers are separated only by ~60 nm.[55] This distance is comparable with a ~ 70 nm distance between the two αC domains within one Fg molecule observed in our MD simulations (Figure 7C). Hence, at higher concentrations the αC regions are capable of forming a network of noncovalent linkages (bonds) between adjacent Fg monomers. The αC regions can also interlock through the excluded volume interactions as shown in Figure 7. These effects result in a dramatic slowdown of molecular diffusion in semidilute and concentrated solutions of full-length Fg, but not in semidilute solutions of des-αC Fg or Fg I-9.

Thermodynamic Basis for the Hydrodynamic Behavior of Fg. Thermodynamically, the intermolecular associations between the αC-domains and between the αC-domain and the central globule are more favorable than the intramolecular associations between these structural elements but in the same Fg molecule, because the former arrangement increases entropy. Since the strength of intra- and intermolecular noncovalent bonds between the αC-domains and between the αC-domains and the central globule are roughly equal,[16] this process is largely entropy-driven. In addition, formation of entangled interlocked aggregates via excluded volume interactions also drives this process, owing to the associated entropy increase. On the other hand, extended forms of the αC-connectors and the straight arrangement of the Fg backbone are less entropically favorable, especially when mean-square diffusive displacements are concerned, and so the αC-connectors tend to adopt a compact structure while the Fg backbone tends to bend. These arguments help to recreate a physical picture underlying the Fg molecular entanglement. In dilute solutions, the average intermonomer distance is long compared to the size of Fg monomers plus the average distance spanned by the αC regions, so Fg molecules experience diffusive displacements within their own pervaded volumes. The intermonomer separation decreases with increasing concentration, and in ~5–10 μM solutions this separation distance is comparable with the combined dimension of the Fg backbone plus the αC regions. The αC regions fluctuating between the compact and extended conformations self-associate intermolecularly thereby pulling on the distal globular D regions and straightening Fg molecules. The binding interactions of the αC regions with the central region of fibrinogen are relatively weak,[16] so there is an equilibrium between bound and dissociated αC regions.[13,15] Some of the intermolecular interactions that we observe here at high concentrations could be these specific αC-αC complexes. This results in mechanical unbending of the Fg backbone, which also tends to interconvert between the extended and bent forms. At each concentration, the tendency of the αC regions to form a compact structure and the propensity of the Fg backbone to bend are balanced, which results in an equilibrium configuration of the matrix of self-assembled Fg monomers in solution.

Alternative Mechanisms of Fg Self-Association. The propensity of Fg molecules to self-assemble has been shown in numerous experiments with chilling (Cohen et al., 1966) and high-speed centrifugation (Stryer et al., 1963), but the underlying mechanism remained elusive. Remarkably, the gels formed by Fg without thrombin-induced conversion to monomeric fibrin displayed highly ordered paracrystalline structures indistinguishable from the fibrin polymers by transmission electron microscopy and X-ray diffraction.[56−59] Hence, the ability of Fg to self-assemble into a regularly packed supramolecular structure without enzymatic cleavage indicates that there are fundamental structural determinants that drive specific association of Fg molecules in semidilute and concentrated solutions. In addition to noncovalent interactions made possible by the αC regions, direct intermolecular coupling between the D regions of adjacent Fg molecules might provide an additional mechanism for Fg oligomerization and intermolecular entanglement, but only in more concentrated solutions. The D−D interface comprising γ275−300 residues of Fg can mediate the end-to-end junction between Fg molecules in the same fashion as the D−D interaction dependent end-to-end junction between fibrin monomers occurs.[60] That the D−D interactions reinforced by covalent cross-linking in semidiluted Fg solutions (10 mg/mL) result in formation of linear Fg oligomers, has been visualized using transmission electron microscopy.[4,61] Another conceivable mechanism for Fg bending and self-association in concentrated solutions is the intermolecular binding between the N-termini of Fg Bβ chains and the central E region in the same or two different Fg molecules.[62]

CONCLUSIONS

This work provides quantitative characteristics of the molecular hydrodynamics of a physiologically important protein, fibrinogen (Fg), obtained using high-resolution NMR diffusometry. These characteristics include the temperature and concentration dependence of the self-diffusion coefficient, reflecting an unusual structure and solution properties of this important biopolymer. When Fg concentration increases from dilute solutions to a more concentrated range, the diffusive motion undergoes a remarkable slowdown due to intermolecular entanglement mediated by the extendable polypeptide chains emanating from the Fg backbone called the αC regions. Fg also changes molecular shape from the bent structure in dilute solutions to the elongated structure in semidiluted and concentrated solutions. The results obtained illuminate the importance of Fg self-assembly in modulating the hydrodynamic properties of semidiluted and concentrated Fg preparations, and also point to the potential role of Fg self-assembly in biological and clinical applications.

AUTHOR INFORMATION

Corresponding Authors
*Tel.: +7-843-231-9036; Fax: +7-843-292-7347; E-mail: yufzuev@mail.ru.
*Tel.: +1-215-898-3573; Fax: +1-215-898-9871; E-mail: weisel@mail.med.upenn.edu.

ORCID
Artem Zhmurov: 0000-0002-4414-8352

Author Contributions
Y.F.Z., R.I.L., and J.W.W. designed research, analyzed data, and wrote the article; Y.F.Z., B.Z.I., D.R.B., D.K.G., and A.Z. performed research; and A.E.S. and V.B. analyzed and modeled data, and wrote the article.

Notes
The authors declare no competing financial interest.

■ ACKNOWLEDGMENTS

■ ABBREVIATIONS:

D-self-diffusion coefficient; D_0-self-diffusion coefficient extrapolated to the infinite protein dilution; Fg-fibrinogen; NMR-nuclear magnetic resonance; MWCO-molecular weight cutoff; DOSY-diffusion-ordered spectroscopy

■ REFERENCES

(1) Weisel, J. W.; Litvinov, R. I. Fibrin Formation, Structure and Properties. In *Fibrous Proteins: Structures and Mechanisms*; Parry, D. A. D., Squire, J. M., Eds.; Springer International Publishing, 2017; Vol. 82, pp 405−456.

(2) Corral, M.; Ferko, N.; Hollmann, S.; Hogan, A.; Jamous, N.; Batiller, J.; Shen, J. Clinician Reported Ease of Use for a Novel Fibrin Sealant Patch for Hemostasis: Results from Four Randomized Controlled Trials. *Curr. Med. Res. Opin.* 2016, 32, 367−375.

(3) Mosesson, M. W.; Siebenlist, K. R.; Hainfeld, J. F.; Wall, J. S. The Covalent Structure of Factor XIIIa Crosslinked Fibrinogen Fibrils. *J. Struct. Biol.* 1995, 115, 88−101.

(4) Fowler, W. E.; Erickson, H. P. Trinodular Structure of Fibrinogen: Confirmation by Both Shadowing and Negative Stain Electron Microscopy. *J. Mol. Biol.* 1979, 134, 241−249.

(5) Williams, R. C. Morphology of Bovine Fibrinogen Monomers and Fibrin Oligomers. *J. Mol. Biol.* 1981, 150, 399−408.

(6) Weisel, J. W.; Stauffacher, C. V.; Bullitt, E.; Cohen, C. A Model for Fibrinogen: Domains and Sequence. *Science* 1985, 230, 1388−1391.

(7) Kollman, J. M.; Pandi, L.; Sawaya, M. R.; Riley, M.; Doolittle, R. F. Crystal Structure of Human Fibrinogen. *Biochemistry* 2009, 48, 3877−3886.

(8) Yee, V. C.; Pratt, K. P.; Côté, H. C.; Le Trong, I.; Chung, D. W.; Davie, E. W.; Stenkamp, R. E.; Teller, D. C. Crystal Structure of a 30 kDa C-terminal Fragment From the γ-Chain of Human Fibrinogen. *Structure* 1997, 5, 125−138.

(9) Spraggon, G.; Everse, S. J.; Doolittle, R. F. Crystal Structures of Fragment D From Human Fibrinogen and its Crosslinked Counterpart From Fibrin. *Nature* 1997, 389, 455−462.

(10) Brown, J. H.; Volkmann, N.; Jun, G.; Henschen-Edman, A. H.; Cohen, C. The Crystal Structure of Modified Bovine Fibrinogen. *Proc. Natl. Acad. Sci. U. S. A.* 2000, 97, 85−90.

(11) Madrazo, J.; Brown, J. H.; Litvinovich, S.; Dominguez, R.; Yakovlev, S.; Medved, L.; Cohen, C. Crystal Structure of the Central Region of Bovine Fibrinogen (E5 Fragment) at 1.4-Å Resolution. *Proc. Natl. Acad. Sci. U. S. A.* 2001, 98, 11967−11972.

(12) Tsurupa, G.; Tsonev, L.; Medved, L. Structural Organization of the Fibrin(ogen) αC-Domain. *Biochemistry* 2002, 41, 6449−6459.

(13) Veklich, Y. I.; Gorkun, O. V.; Medved, L. V.; Nieuwenhuizen, W.; Weisel, J. W. Carboxyl-terminal Portions of the Alpha Chains of Fibrinogen and Fibrin. Localization by Electron Microscopy and the Effects of Isolated Alpha C Fragments on Polymerization. *J. Biol. Chem.* 1993, 268, 13577−13585.

(14) Protopopova, A. D.; Barinov, N. A.; Zavyalova, E. G.; Kopylov, A. M.; Sergienko, V. I.; Klinov, D. V. Visualization of Fibrinogen αC Regions and Their Arrangement During Fibrin Network Formation by High-resolution AFM. *J. Thromb. Haemostasis* 2015, 13, 570−579.

(15) Weisel, J. W.; Medved, L. V. The Structure and Function of the αC Domains of Fibrinogen. *Ann. N. Y. Acad. Sci.* 2001, 936, 312−327.

(16) Litvinov, R. I; Yakovlev, S.; Tsurupa, G.; Gorkun, O. V.; Medved, L.; Weisel, J. W. Direct Evidence for Specific Interactions of the Fibrinogen αC-Domains with the Central E Region and with Each Other. *Biochemistry* 2007, 46, 9133−9142.

(17) Raynal, B.; Cardinali, B.; Grimbergen, J.; Profumo, A.; Lord, S. T.; England, P.; Rocco, M. Hydrodynamic Characterization of Recombinant Human Fibrinogen Species. *Thromb. Res.* 2013, 132, e48−e53.

(18) Martinez, M. C. L.; Rodes, V.; de la Torre, J. G. Estimation of the Shape and Size of Fibrinogen in Solution from its Hydrodynamic Properties Using Theories for Bead Models and Cylinders. *Int. J. Biol. Macromol.* 1984, 6, 261−265.

(19) Cardinali, B.; Profumo, A.; Aprile, A.; Byron, O.; Morris, G.; Harding, S. E.; Stafford, W. F.; Rocco, M. Hydrodynamic and Mass Spectrometry Analysis of Nearly-intact Human Fibrinogen, Chicken Fibrinogen, and of a Substantially Monodisperse Human Fibrinogen Fragment X. *Arch. Biochem. Biophys.* 2010, 493, 157−168.

(20) Wasilewska, M.; Adamczyk, Z. Fibrinogen Adsorption on Mica Studied by AFM and in Situ Streaming Potential Measurements. *Langmuir* 2011, 27, 686−696.

(21) Adamczyk, Z.; Cichocki, D.; Ekiel-Jeżewska, M. L.; Słowicka, A.; Wajnryb, E.; Wasilewska, M. Fibrinogen Conformations and Charge in Electrolyte Solutions Derived from DLS and Dynamic Viscosity Measurements. *J. Colloid Interface Sci.* 2012, 385, 244−257.

(22) Price, W. S. *NMR Studies of Translational Motion. Principles and Application*; Cambridge University Press: Cambridge, 2009.

(23) Price, W. S. NMR Gradient Methods in the Study of Proteins. *Annu. Rep. Prog. Chem., Sect. C: Phys. Chem.* 2000, 96, 3−53.

(24) Nesmelova, I. V.; Skirda, V. D.; Fedotov, V. D. Generalized Concentration Dependence of Globular Protein Self-diffusion Coefficient in Aqueous Solutions. *Biopolymers* 2002, 63, 132−140.

(25) Mutina, A. R.; Skirda, V. D. Rodlike Polymer Gelatination as Studied by PFG NMR: Fibrin Polymerization in Human Plasma. *Appl. Magn. Reson.* 2004, 27, 527−538.

(26) Mosesson, M. W.; Galanakis, D. K.; Finlayson, J. S. Comparison of Human Plasma Fibrinogen Subfractions and Early Plasmic Fibrinogen Derivatives. *J. Biol. Chem.* 1974, 249, 4656−4664.

(27) Mosesson, M. W.; Alkjaersig, N.; Sweet, B.; Sherry, S. Human Fibrinogen of Relatively High Solubility. Comparative Biophysical, Biochemical, and Biological Studies with Fibrinogen of Lower Solubility. *Biochemistry* 1967, 6, 3279−3287.

(28) Wu, D. H.; Chen, A. D.; Johnson, C. S. An Improved Diffusion-Ordered Spectroscopy Experiment Incorporating Bipolar-Gradient Pulses. *J. Magn. Reson., Ser. A* 1995, 115, 260−264.

(29) Hoye, T. R.; Eklov, B. M.; Ryba, T. D.; Voloshin, M.; Yao, L. J. No-D NMR (No-Deuterium Proton NMR) Spectroscopy: A Simple Yet Powerful Method for Analyzing Reaction and Reagent Solutions. *Org. Lett.* 2004, 6, 953−956.

(30) Humphrey, W.; Dalke, A.; Schulten, K. VMD - Visual Molecular Dynamics. *J. Mol. Graphics* 1996, 14, 33−38.

(31) Šali, A.; Blundell, T. L. Comparative Protein Modelling by Satisfaction of Spatial Restraints. *J. Mol. Biol.* 1993, 234, 779−815.

(32) Burton, R. A.; Tsurupa, G.; Hantgan, R. R.; Tjandra, N.; Medved, L. NMR Solution Structure, Stability, and Interaction of the Recombinant Bovine Fibrinogen αC-Domain Fragment. *Biochemistry* 2007, 46, 8550−8560.

(33) Ferrara, P.; Apostolakis, J.; Caflisch, A. Evaluation of a Fast-Implicit Solvent Model for Molecular Dynamics Simulations. *Proteins: Struct., Funct., Genet.* 2002, 46, 24−33.

(34) Zhmurov, A.; Kononova, O.; Litvinov, R. I.; Dima, R. I.; Barsegov, V.; Weisel, J. W. Mechanical Transition From α-helical Coiled coils to β-sheets in Fibrin(ogen). *J. Am. Chem. Soc.* 2012, 134, 20396−20402.

(35) Zhmurov, A.; Brown, A. E.; Litvinov, R. I.; Dima, R. I.; Weisel, J. W.; Barsegov, V. Mechanism of Fibrin (ogen) Forced Unfolding. *Structure* **2011**, *19*, 1615−1624.

(36) Monkos, K. A. Comparison of the Activation Energy of Viscous Flow for Hen Egg-white Lysozyme Obtained on the Basis of Different Models of Viscosity for Glass-forming Liquids. *Curr. Top. Biophys* **2011**, *34*, 1−9.

(37) Tanaka, K. Measurements of Self-diffusion Coefficient of Water in Pure Water and in Aqueous Electrolyte Solutions. *J. Chem. Soc., Faraday Trans. 1* **1975**, *71*, 1127−1131.

(38) Medved, L. V.; Weisel, J. W. Recommendations for Nomenclature on Fibrinogen and Fibrin. *J. Thromb. Haemostasis* **2009**, *7*, 355−359.

(39) Laudano, A. P.; Cottrell, B. A.; Doolittle, R. F. Synthetic Peptides Modeled on Fibrin Polymerization Sites. *Ann. N. Y. Acad. Sci.* **1983**, *408*, 315−329.

(40) Chernysh, I. N.; Nagaswami, C.; Purohit, P. K.; Weisel, J. W. Fibrin Clots Are Equilibrium Polymers That Can Be Remodeled Without Proteolytic Digestion. *Sci. Rep.* **2012**, *2*, 879−884.

(41) Tokuyama, M.; Oppenheim, I. Dynamics of Hard-sphere Suspensions. *Phys. Rev. E: Stat. Phys., Plasmas, Fluids, Relat. Interdiscip. Top.* **1994**, *50*, R16−R19.

(42) Asadi, M. *Beet-Sugar Hand Book*; John Wiley and Sons Ltd: UK, 2007.

(43) Rubinstein, M.; Colby, R. *Polymer Physics*; Oxford University Press: Oxford, 2012.

(44) Weast, R. C.; Astle, M. J.; Beyer, W. H. *CRC Handbook of Chemistry and Physics*; CRC press: Boca Raton, FL, 1988.

(45) Tsao, T. C.; Bailey, K.; Adair, G. S. The Size, Shape and Aggregation of Tropomyosin Particles. *Biochem. J.* **1951**, *49*, 27.

(46) Shulman, S. The Size and Shape of Bovine Fibrinogen. Studies of Sedimentation, Diffusion and Viscosity. *J. Am. Chem. Soc.* **1953**, *75*, 5846−5852.

(47) Lederer, K.; Schurz, J. High Shear Rate Viscosity Measurements with Dilute Solutions of Bovine Fibrinogen. *Biopolymers* **1972**, *11*, 1989−1993.

(48) Nemoto, N.; Nestler, F. H. M.; Schrag, J. L.; Ferry, J. D. Infinite-dilution Viscoelastic Properties of Fibrinogen and Intermediate Fibrin Polymer. *Biopolymers* **1977**, *16*, 1957−1969.

(49) Armstrong, J. K.; Wenby, R. B.; Meiselman, H. J.; Fisher, T. C. The Hydrodynamic Radii of Macromolecules and their Effect on Red Blood Cell Aggregation. *Biophys. J.* **2004**, *87*, 4259−4270.

(50) Gaigalas, A. K.; Hubbard, J. B.; McCurley, M.; Woo, S. Diffusion of Bovine Serum Albumin in Aqueous Solutions. *J. Phys. Chem.* **1992**, *96*, 2355−2359.

(51) Köhler, S.; Schmid, F.; Settanni, G. The Internal Dynamics of Fibrinogen and Its Implications for Coagulation and Adsorption. *PLoS Comput. Biol.* **2015**, *11*, e1004346.

(52) Tsurupa, G.; Hantgan, R. R.; Burton, R. A.; Pechik, I.; Tjandra, N.; Medved, L. Structure, Stability, and Interaction of the Fibrin(ogen) *αC*-domains. *Biochemistry* **2009**, *48*, 12191−12201.

(53) Burton, R. A.; Tsurupa, G.; Medved, L.; Tjandra, N. Identification of an Ordered Compact Structure within the Recombinant Bovine Fibrinogen *αC*-Domain Fragment by NMR. *Biochemistry* **2006**, *45*, 2257−2266.

(54) Pamies, R.; Cifre, J. G. H.; Martínez, M. D. C. L.; de la Torre, J. G. Determination of Intrinsic Viscosities of Macromolecules and Nanoparticles. Comparison of Single-point and Dilution Procedures. *Colloid Polym. Sci.* **2008**, *286*, 1223−1231.

(55) Erickson, H. P. Size and Shape of Protein Molecules at the Nanometer Level Determined by Sedimentation, Gel Filtration, and Electron Microscopy. *Biol. Proced. Online* **2009**, *11*, 32−51.

(56) Stryer, L.; Cohen, C.; Langridge, R. Axial Period of Fibrinogen and Fibrin. *Nature* **1963**, *197*, 793−794.

(57) Cohen, C.; Slayter, H.; Goldstein, L.; Kucera, J.; Hall, C. Polymorphism in Fibrinogen Aggregates. *J. Mol. Biol.* **1966**, *22*, 385−386.

(58) Gollwitzer, R.; Bode, W.; Schramm, H.-J.; Typke, D.; Guckenberger, R. Laser Diffraction of Oriented Fibrinogen Molecules. *Ann. N. Y. Acad. Sci.* **1983**, *408*, 214−225.

(59) Stewart, G. J.; Niewiarowski, S. Nonenzymatic Polymerization of Fibrinogen by Protamine Sulfate An Electron Microscope Study. *Biochim. Biophys. Acta, Protein Struct.* **1969**, *194*, 462−469.

(60) Zhmurov, A.; Protopopova, A. D.; Litvinov, R. I.; Zhukov, P.; Mukhitov, A. R.; Weisel, J. W.; Barsegov, V. Structural Basis of Interfacial Flexibility in Fibrin Oligomers. *Structure* **2016**, *24*, 1907−1917.

(61) Brown, A. E. X.; Litvinov, R. I.; Discher, D. E.; Weisel, J. W. Forced Unfolding of Coiled-Coils in Fibrinogen by Single-Molecule AFM. *Biophys. J.* **2007**, *92*, L39−L41.

(62) Gorkun, O. V.; Litvinov, R. I.; Veklich, Yu. I.; Weisel, J. W. Interactions Mediated by the N-Terminus of Fibrinogen's B*β* Chain. *Biochemistry* **2006**, *45*, 14843−14852.